JCTC Journal of Chemical Theory and Computation

Establishing Effective Simulation Protocols for β- and α/β-Mixed Peptides. I. QM and QM/MM Models

Xiao Zhu, Arun Yethiraj,* and Qiang Cui*

Department of Chemistry and Theoretical Chemistry Institute, University of Wisconsin—Madison, 1101 University Avenue, Madison, Wisconsin 53706

Received December 18, 2006

Abstract: A quantum mechanical (QM) model for non-natural β- and α/β-mixed peptides is investigated using an approximate density functional method (called SCC-DFTB). In the gas phase the predictions of the model for cyclic and acyclic dipeptides and several acyclic heptapeptides are compared to ab initio B3LYP and LMP2 calculations. The SCC-DFTB reproduces the global minimum of the configurations with the root-mean-square (rms) error in the key dihedral angles of less than 14 degrees. The relative energies of different conformers are also well described in general, with the typical rms error of 2−3 kcal/mol relative to LMP2 energies at either B3LYP or LMP2 optimized structures. The dipole moments are reproduced with a systematic underestimate of less than 15%. The QM model is also used with a molecular mechanical (MM) model of the solvent. For a tetrameric α/β-peptide in water, the SCC-DFTB/MM energies are well correlated with B3LYP/6-31+G**/MM single point energies for a wide range of structures sampled in 2 ns of SCC-DFTB/MM molecular dynamics. For an octameric α/β-peptide in methanol the predicted structures are in qualitative agreement with experimental NOE data. These results suggest that the SCC-DFTB model provides a fairly accurate representation of the structure and thermodynamics of these peptides.

I. Introduction

The primary building blocks of naturally occurring α-peptides are amino acid residues which consist of a peptide bond and an α-carbon atom which can have a side chain. In β-peptides there is an additional carbon atom along the peptide backbone. The presence of two carbon atoms allows one to introduce cyclic residues along the backbone, something that is not possible in α-peptides. This class of relatively new materials has attracted enormous interest lately. This interest derives partly from their unique structural properties and partly from their potential in biomedical and material applications. β-Peptides and α/β-mixed peptides are interesting from a structural perspective because they form secondary structures (e.g., helices, sheets, reverse turns) more readily than natural α-peptides.[1−10] They provide an interesting alternative to conventional peptides in many applications and have the advantage that there is no mechanism in the body for their degradation. Non-natural peptides may have applications as antimicrobial materials[11−16] and gene delivery agents[17] and are possible candidates for lung surfactant mimics. Barron and co-workers[18] have shown that designed peptoid oligomers (N-alkyl-glycine oligomers) can function as lung surfactant mimics. From a fundamental standpoint, the ability to control the chemical composition of non-natural peptides provides a unique opportunity for exploring the role of microscopic properties (e.g., chain stiffness) in determining the phase behavior and other macroscopic properties of polymeric materials.

A central question is the relation between structure and property in these materials. Characterizing the structure of these molecules experimentally is challenging, and quantitative structural information is scarce. There are significant thermal fluctuations in the structure, and this makes the interpretation of, e.g., Nuclear Overhauser Effect (NOE) and Circular Dichroism (CD) experiments far from straightforward.[19] Therefore, much remains to be learned regarding how

* Corresponding author e-mail: yethiraj@chem.wisc.edu (A.Y.) and cui@chem.wisc.edu (Q.C.).

10.1021/ct600352e CCC: $37.00
Published on Web 05/08/2007

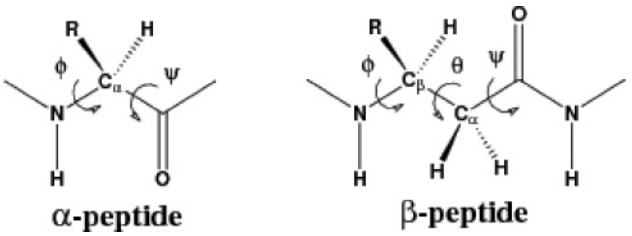

Figure 1. Comparison of α-(left) and β-(right) peptides. The torsional angles essential for characterizing the backbone structure of the system are ϕ and ψ for α-peptides and ϕ, θ, and ψ for β-peptides.

the structure and dynamics of β-peptides depend on their sequence. The goal of our research is to develop accurate models that can predict the structure of peptides in solution from first principles calculations. In this paper we investigate an approximate quantum mechanical (QM) model for non-natural peptides in the gas phase and, using this result, study a hybrid quantum mechanical/classical mechanical (QM/MM) model for peptides in solution.

There have been several experimental studies on the structure of β-peptides[4−8,14,20−23] and α/β-mixed peptides,[9,10] and these have led to some tentative empirical rules relating sequence to structure. For example, the 14-helix (the number 14 refers to the number of atoms between the two hydrogen-bonded moieties) is a preferred conformation for β^3-peptides in organic solvents,[7,20] and cyclic residues in general can greatly enhance the helical propensity of non-natural peptides.[4−6,10] Electrostatic interactions in the forms of intrahelical salt-bridges[21,22] and helical dipoles[24] enhance the stability of 14-helix structures in water. Despite these advances, for the reasons mentioned above, quantitative experimental data are not common, and some of these rules are not universally accepted. For example, β^3-residues that bear a side-chain branch point adjacent to the backbone, such as β^3-Val, have been suggested[24,25] to promote helix formation, but this idea has also been challenged.[26] For α/β-mixed peptides, even less systematic work has been carried out.[27]

The goal of this research is to use molecular simulation to provide a deeper understanding of the sequence-structure−property relations of β- and α/β-peptides. We would like to be able to predict the structure of short β- and α/β-mixed peptides based only on sequence information, and, once the structure of individual peptide is known, we would like to be able to predict the macroscopic material properties of solutions of these peptides. Ultimately, we hope to use computational methods to aid the design of non-natural peptides with desired structure and function, e.g., as lung surfactant mimics.

There have been a few computational studies of β-peptides using ab initio QM calculations[28−30] and molecular dynamics (MD) simulations using classical force fields.[31−35] The ab initio calculations are valuable benchmarks but far too computationally intensive to map out the conformational and sequence space of interest. Classical MD simulations are computationally convenient but employ empirical force fields the parameters of which must be determined by comparison to either high level ab initio QM calculations or experiment. Most previous classical MD simulations employed force field parameters developed for the α-amino acids which are probably not transferable to non-natural peptides. Therefore, although those studies provide valuable qualitative insight, they are not expected to be quantitatively reliable. Indeed, quantitatively validating the force field for non-natural peptides is not straightforward because experimental data are limited, and high level QM calculations are available only for the gas phase; most force fields are developed for peptides in solution.[36]

A useful compromise, which we have decided to follow, is a hierarchical protocol in which both hybrid quantum mechanical/classical mechanical (QM/MM)[37−40] and classical molecular mechanics (MM) simulations are used. In particular, we use QM/MM simulations as the reference to facilitate the development of a reliable MM force field for peptides that contain β-amino acids. In cases where larger-scale simulations (e.g., for the study of phase behaviors) are needed, the all-atom MM simulations can be used to parametrize an effective coarse-grained model. The reason to use a QM/MM model is that a QM model, in contrast to a MM model, can be directly calibrated against high-level ab initio calculations in the gas phase, which makes QM/MM simulations a uniquely meaningful reference.

Computational considerations force us to use an approximate QM model, and we use the Self-Consistent-Charge Density Functional Tight Binding (SCC-DFTB) method.[41] Our choice is motivated by the computational efficiency of this method (comparable to widely used semiempirical methods such as AM1 and PM3) coupled with its reasonable accuracy, especially concerning the treatment of hydrogen bonding interactions.[42] The SCC-DFTB method has been applied successfully to a range of problems involving biomolecules, such as conformational energies of natural peptides[43−45] and catalysis in several enzymes;[46−49] a recent review can be found in ref 50. Furthermore, the SCC-DFTB approach has been benchmarked for reaction energies, geometries, and vibrational frequencies for small molecules in comparison to the G2 approach.[51] An empirical dispersion correction has also been developed,[52] which was found to be crucial for predicting reliable nucleic acid base-stacking interactions[52] and the relative stability of α and 3_{10} helices in proteins.[53]

In this work, we set out to check the validity of SCC-DFTB as an appropriate QM method for β- and α/β-peptides with a diverse set of benchmark calculations, which include analyses in both the gas phase and in solution (methanol, water). In the gas phase, we test the method by comparison to high level ab initio calculations; in solution, we test the method by comparison to available experiments or QM/MM simulations with a high-level QM method. We find that the SCC-DFTB method is an acceptable alternative to high-level QM methods. The optimized structures are consistent with high level calculations, the barriers in the torsoinal potential energy are different by ∼2−4 kcal/mol, and the dipole moments are within 15% of the high level calculations. Similar agreement is also found in solution.

The rest of the paper is organized as follows. The computational methods are described in section 2, the results

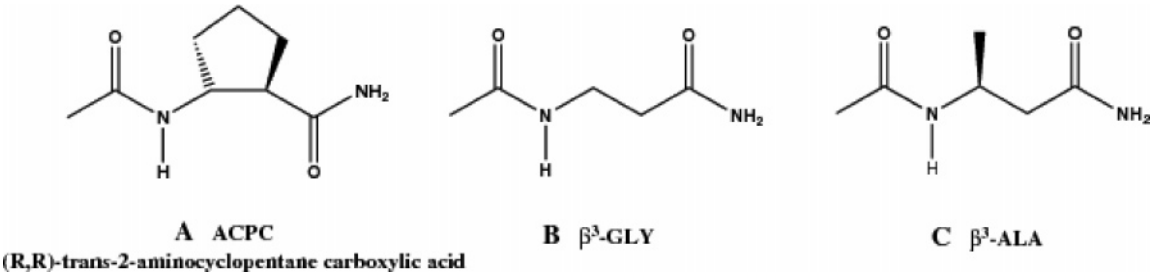

Figure 2. Dipeptide models studied here in the gas phase: **A**(ACPC), **B**(β^3-GLY), and **C**(β^3-ALA).

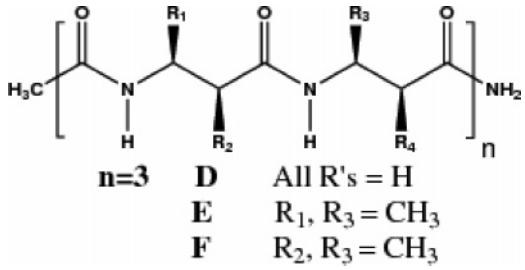

Figure 3. The heptapeptide models studied here in the gas phase: **D**−**F**.

are presented and discussed in section 3, and some conclusions are presented in section 4.

II. Methods

We test the performance of the SCC-DFTB method for peptides containing β-amino acids with benchmark calculations in the gas phase and in solution. The SCC-DFTB results for β-peptides in the gas phase are compared to high-level density functional theory (DFT)[54] and local MP2 calculations (LMP2).[55] The predictions of the method, implemented in a QM/MM framework,[46] for α/β-mixed peptides in water and methanol are compared to DFT/MM simulations and experiments, respectively. This section describes the nomenclature and methodology used in these calculations.

A. β-Peptides in the Gas Phase. *1. One-Dimensional Adiabatic Mapping.* Since β-amino acids have an additional carbon atom along the backbone, compared to α-amino acids, we require one more torsional angle to describe the backbone conformation. In addition to the usual ϕ-ψ torsional angles, we require the angle (denoted θ) for the rotation along the $C_\alpha-C_\beta$ bond (Figure 1). As the first set of benchmark calculations, one-dimensional adiabatic mapping along these three degrees of freedom is carried out for two simple β dipeptides (**A** and **C** in Figure 2) at different levels of quantum mechanical theories; these include the standard SCC-DFTB,[41] Hartree−Fock (HF) with the 6-31G* basis set,[56] B3LYP[57−59] with the 6-31+G** basis set, and LMP2 with a larger 6-311G** basis set.[60] Diffuse functions have been included in the B3LYP calculations, because it has been shown that basis set superposition error (BSSE) for hydrogen-bonding interactions and conformational energies is reduced significantly with diffuse functions.[61,62] The LMP2 rather than the canonical MP2 calculations are chosen because of the lower computational cost and reduced BSSE for the LMP2 approach;[63] previous calculations[64,65] showed that LMP2 with triplet-zeta plus polarization basis sets perform accurately for conformational energies of natural peptides. The adiabatic energy profile is calculated every 18° for each torsional angle, which spans the entire 360° range except that θ in compound **C** only goes from −180° to 0° due to stereochemical constraints.

2. Conformational Studies of Model Peptides. To sample the conformations of dipeptides more extensively, a systematic conformational search with 30° increments for the three characteristic dihedral angles (ϕ, ψ, θ) is performed for β^3-GLY and β^3-ALA (**B** and **C** in Figure 2). This generates a total of 1728 starting structures for each compound, which are then subject to minimization at different levels of theories: SCC-DFTB, B3LYP/6-31+G**, and LMP2/6-31G**; for SCC-DFTB, in addition to the standard parametrization, a recently proposed model for improving hydrogen-bonding interactions (referred to as "Hbond" parametrization in tables[66,67]) and an empirical dispersion correction[68] have also been tested. Following the structural optimizations, single point energies are evaluated at the LMP2 level with a larger 6-311G** basis set;[60] dipole moments are also calculated with the standard SCC-DFTB and B3LYP/6-31+G**. The motivation of including the local MP2 results is that dispersion interactions, which have been found necessary for properly describing the relative stability of α-helix and 3_{10}-helix of natural peptides,[69] are poorly described in the popular DFT methods such as B3LYP.[68−70] It is possible that dispersion could possibly make an important contribution to the relative stability of different conformers for β-peptides.

In addition to the simple dipeptides, several more complex heptapeptide molecules that have been analyzed in previous studies are also considered (Figure 3). The quantity of interest is the relative stability of the 14-helix and two different 10/12 mixed helical structures.[2] These conformations are fully optimized at both the SCC-DFTB and B3LYP/6-31G* levels. Similar to the dipeptide studies, single point energies of the optimized conformers are also calculated at the LMP2/6-311G** level, and the dipole moments are calculated with the standard SCC-DFTB and B3LYP/6-31+G**.

All HF and DFT calculations are carried out using the GAUSSIAN 03 package[71] and LMP2 calculations using Jaguar.[72] In all SCC-DFTB optimizations, the Adapted Basis Newton−Raphson (ABNR) approach in CHARMM[73] is used with a gradient tolerance of 0.0001 kcal/(mol·Å) for the dipeptides and 0.001 kcal/(mol·Å) for the heptapeptides.

B. α/β-Mixed Peptides in the Condensed Phase. Two sequences of α/β-mixed peptides are studied in the condensed phase, with the QM/MM approach, and these are depicted in Figure 4. The tetrapeptide (ACPC-A-ACPC-A, where

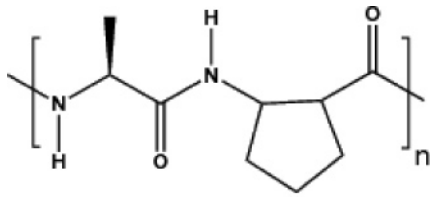

Figure 4. The α/β-mixed peptide models studied here in solution; the tetra- ($n = 2$) and octapeptides ($n = 4$), which are studied in water and methanol, respectively.

ACPC is (*R,R*)-*trans*-2-aminocyclopentane carboxylic acid) is studied in aqueous solution, and the initial structure is built from the crystal structure for a slightly different system[10] where the α-amino acids are Aib. The octapeptide (ACPC-A-ACPC-A-ACPC-A-ACPC-A) is studied in methanol, and the starting configuration is built from the NOE derived structure reported by Schmitt et al.[10] In both studies, the peptide is treated with QM, and the solvent (water or methanol) is treated with a MM model.

1. Tetrapeptide (ACPC-A-ACPC-A) in Explicit Water. Molecular dynamics simulations are carried out with SCC-DFTB/MM[74] at 300 K. The peptide is treated with the standard SCC-DFTB, while the solvent molecules are treated classically using the TIP3P model.[75] The peptide is solvated in an 18 Å water sphere, and the generalized solvent boundary potential (GSBP)[76,77] is used for the boundary condition with a 2 Å water exclusion radius.[76] The system contains a total of 549 TIP3P water molecules and 65 peptide atoms. Two nanoseconds of equilibrium QM/MM simulation are carried out in which atoms in the spherical shell from 13 to 16 Å are treated with Langevin dynamics while the rest with Newtonian dynamics.[78] A time step of 1.0 fs is used, and all bonds to hydrogen atoms are constrained with SHAKE.[79]

To evaluate the accuracy of the SCC-DFTB/MM hybrid potential, ~70 snapshots are taken from the 2 ns QM/MM simulation, and single point energy calculations are performed at the B3LYP/6-31+G**/MM level with the GAMESS package[80] interfaced with CHARMM.

2. Octapeptide (ACPC-A-ACPC-ACPC-A-ACPC-A) in Methanol. In the octapeptide-methanol simulation, the peptide is treated with the standard SCC-DFTB, while the methanol molecules are treated classically using the MEOH model in the CHARMM 22 all-atom force field;[36] calculations show that this methanol model describes the bulk property rather well with both periodic boundary and GSBP simulations (see the Supporting Information). The peptide is solvated in a 20 Å methanol sphere around its center of mass with a 2.5 Å of methanol exclusion shell associated with the GSBP setup. The system contains a total of 357 MEOH methanol molecules and 117 peptide atoms.

For the octapeptide, the issue of interest is the relative stability of the 14/15 and 11 helical structures. NOE data in methanol suggest that both conformers appear with likely similar stability.[10] Motivated by this observation, the potential of mean force (PMF) associated with the conversion between the two helical forms is calculated using umbrella sampling.[81] The reaction coordinate is chosen to be the end-to-end distance between the amide nitrogen in the first residue and the carbonyl carbon in the last residue, and the sampled range is between 10.6 and 18.0 Å. To prepare the initial structures for the umbrella samplings, a 14/15-helix is pulled toward the 11-helix in the gas phase with the reaction coordinate and intermediate structures collected every 0.2 Å, which are then used as the starting peptide conformation for each window. Totally 37 windows are sampled, each including 25 ps of equilibration and 75 ps of production calculations. The Weighted Histogram Analysis Method (WHAM)[82] is used to analyze the data to obtain the PMF.

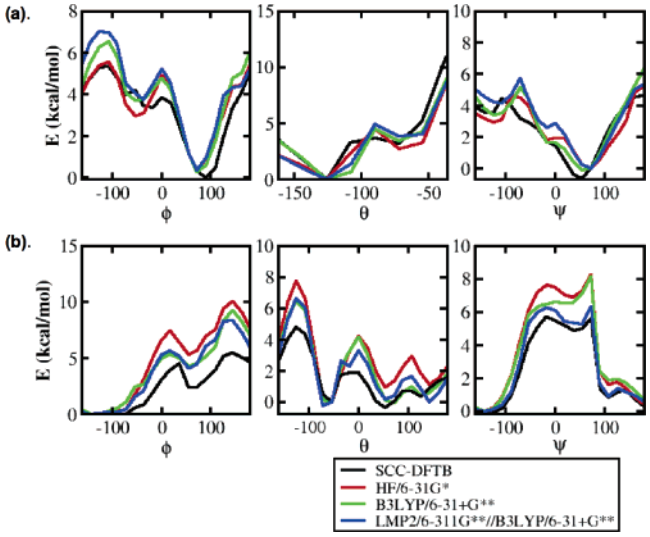

Figure 5. One-dimensional adiabatic energy map along the torsional angles ϕ, θ, and ψ for the (a) cyclic dipeptide **A** and (b) acyclic dipeptide **C**. Black: standard SCC-DFTB; red: HF/6-31G*; green: B3LYP/6-31+G**; blue: LMP2/6-311G**//B3LYP/6-31+G**.

III. Results and Discussions

A. β-Peptides in the Gas Phase. *1. One-Dimensional Adiabatic Mapping of a Dipeptide.* The SCC-DFTB reproduces the general features of the energy profiles along the ϕ, θ, and ψ angles for both the cyclic and acyclic dipeptides. Figure 5 (a),(b) compares the SCC-DFTB predictions to ab initio (HF, B3LYP, and LMP2) calculations for cylic and acyclic peptides, respectively. The positions of local mimina and maxima are the same in all theories, but the SCC-DFTB tends to underestimate the barriers between different minima, especially in the case of β^3-Ala (which has a more flexible backbone than ACPC). The largest errors are found for the energy profile along ϕ and can be as large as ~3−4 kcal/mol compared to the LMP2 results. In the other cases, the errors are typically smaller than 2 kcal/mol. The implication is that the structure of β-peptides may be too flexible in SCC-DFTB and SCC-DFTB/MM simulations, although the theory is expected to be reliable for the structural *propensity*.

2. Conformational Studies of Dipeptides. For the acyclic dipeptides, β^3-Gly (**B**) and β^3-Ala (**C**), systematic conformational searches have identified six and twelve low-energy conformers, respectively (not including mirror image struc-

Table 1. Dihedral Angles, Dipole Moments, and Relative Energies for Optimized Conformers of Model **B** at Different QM Levels[a]

		dihedral angles (SCC[d])			ΔE					dipole moment	
conformer[b]	type[c]	ϕ	θ	ψ	SCC[d]	SCC-dispersion[e]	SCC-Hbond[f]	B3LYP[g]	LMP2[h]	SCC[d]	B3LYP[g]
B1	C_8	−109.6	56.8	35.4	0.0	0.0	0.0	0.0	0.0	3.6	5.3
B2	C_6	117.5	58.1	125.6	0.3	0.5	0.5	−0.5	0.2	4.8	4.4
B3	C_8	−83.3	124.8	−56.0	0.9	0.9	0.9	1.0	0.9	5.2	6.1
B4	C_8	−46.4	−51.3	110.3	1.4	1.4	1.6	−0.5	0.6	3.1	4.4
B5		−80.5	167.3	−67.6	2.2	0.9	2.8	1.6	0.9	2.9	2.3
B6		−92.9	−171.7	−144.6	2.6	0.9	3.1	1.6	1.7	3.4	2.3

[a] For structure, see Figure 2. Energies are in kcal/mol, dihedral angles in degrees, dipole moment in Debyes. [b] The mirror image conformers are energetically equivalent, and their dihedral angles differ only by sign. [c] C_x: hydrogen-bonded cycles with x atoms. [d] The standard parametrization of SCC-DFTB.[41] [e] SCC-DFTB with the empirical dispersion interaction;[68] both **B5** and **B6** convert to **B3**. [f] SCC-DFTB with the hydrogen-bonding interaction correction.[66,67] [g] Fully optimized at the B3LYP/6-31+G** level; **B4** converts to the mirror image conformer of **B2** and **B5** converts to **B6**. [h] LMP2/6-311G** single point energies at the LMP2/6-31G** optimized structures; **B5** converts to **B3**.

Table 2. Dihedral Angles, Dipole Moments, and Relative Energies for Optimized Conformers of Model **C** at Different QM Levels[a]

		dihedral angles (SCC[c])			ΔE					dipole moment	
conformer	type[b]	ϕ	θ	ψ	SCC[c]	SCC-dispersion[d]	SCC-Hbond[e]	B3LYP[f]	LMP2[g]	SCC[c]	B3LYP[f]
C1	C_8	−109.8	53.0	39.8	0.0	0.0	0.0	0.0	0.0	3.6	5.1
C2	C_6	−106.7	−59.7	−128.6	0.2	0.1	0.4	−0.2	−0.5	4.6	5.4
C3	C_8	−78.2	129.3	−61.4	0.7	0.5	0.6	0.4	0.1	5.1	5.8
C4	C_8	−49.6	−48.6	111.0	1.1	1.1	1.3	1.7	0.4	2.8	2.6
C5	C_6	−167.1	54.3	112.9	1.3	1.3	1.4	1.6	0.9	4.3	4.6
C6	C_6	57.8	58.3	178.4	1.3	1.4	1.5	1.3	2.3	2.0	0.9
C7	C_8	50.2	48.4	−111.2	1.4	1.6	1.6	1.7	0.4	3.0	3.0
C8		−64.0	171.6	−175.9	2.6	0.5	2.9	0.4	0.1	3.5	5.8
C9	C_8	63.7	−126.5	83.4	2.8	2.6	2.8	4.0	3.3	5.0	6.0
C10		60.0	169.3	160.2	2.8	3.0	3.3	3.0	2.6	1.7	1.3
C11	$H_{10/12}$	71.5	−37.0	−94.4	3.3	0.5	3.8	7.8	5.7	2.5	3.5
C12		−173.9	−72.5	42.3	5.1	5.0	5.4	6.3	4.6	3.5	3.0

[a] For structure, see Figure 2. Energies are in kcal/mol, dihedral angles in degrees, dipole moment in Debyes. [b] C_x hydrogen-bonded cycles with x atoms; $H_{x/y}$ mixed helix pattern. [c] The standard parametrization of SCC-DFTB.[41] [d] SCC-DFTB with the empirical dispersion interaction;[68] **C8** converts to **C3** and **C11** to **C5**. [e] SCC-DFTB with the hydrogen-bonding interaction correction.[66,67] [f] Fully optimized B3LYP/6-31+G**; **C8** converts to **C3**. [g] LMP2/6-311G** single point energies at the LMP2/6-31G** optimized structures; **C8** converts to **C3**.

Table 3. rms Differences in Optimized Dihedral Angles in Various β-Peptides Compared to the Standard SCC-DFTB Results[a]

model	SCC-dispersion[c]	SCC-Hbond[d]	B3LYP	LMP2[g]
dipeptide	8.8	6.6	13.4[e]	9.9
heptapeptide[b]	6.7	0.7	9.0[f]	

[a] All dihedral angles rms differences are in degrees. [b] Only the 10/12 mixed helices are included; for the 14-helix, see Figures 6−8. [c] SCC-DFTB with the empirical dispersion interaction.[68] [d] SCC-DFTB with the hydrogen-bonding interaction correction.[66,67] [e] B3LYP/6-31+G**. [f] B3LYP/6-31G*. [g] LMP2/6-31G**.

Table 4. rms Differences in Relative Energetics for Various β-Peptides Compared to LMP2/6-311G** Single Point Energies[a]

model	SCC[d]	SCC-dispersion[e]	SCC-Hbond[f]	B3LYP[g]
dipeptide[b]	1.2	1.3	1.3	0.9
heptapeptide[b]	3.3	4.5	3.6	2.2
heptapeptide[c]	2.0			2.6

[a] All energies are in kcal/mol. [b] With the standard SCC-DFTB optimized structures; for the heptapeptides, only the 10/12 mixed helices and the fully optimized 14-helices are included. [c] With B3LYP/6-31G* optimized structures. [d] The standard parametrization of SCC-DFTB.[41] [e] SCC-DFTB with the empirical dispersion interaction.[68] [f] SCC-DFTB with the hydrogen-bonding interaction correction.[66,67] [g] B3LYP/6-31+G**.

tures for **B**); the structure, energy, and dipole moment of these conformers are summarized in Tables 1 and 2.

For both β-dipeptides, SCC-DFTB is able to reproduce most of the structures predicted by previous ab initio calculations[28,30] and has identified new locally stable structures not reported before. For **B**, conformers **B1, B2, B3**, and **B6** are consistent with those found in previous HF/6-31G** calculations,[28] and **B4** and **B5** have not been reported before. Instead, Wu et al.[28] reported two other conformers, which are not local minima and convert to the lower energy conformer **B1** at *both* SCC-DFTB and B3LYP/6-31+G** levels. For **C**, SCC-DFTB reproduces 8 conformers (**C1, C2, C4, C5, C6, C7, C8, C10**) out of the ten that have been reported by Wu and Wang.[28] Other conformers (**C3, C9, C11, C12**) were found in calculations of Möhle et al.,[30] although their model is N-methylated. One of the two conformers found by Wu et al.[28] converts to **C1** at both SCC-DFTB and B3LYP/6-31+G** levels. The other one converts to **C5** with SCC-DFTB; it is a local minimum at the B3LYP/6-31+G** level although it is much higher in energy than most of the conformers in Table 2 (except for **C11** and **C12**). Overall, the optimized dihedral angles in these low-energy conformers at the SCC-DFTB level are fairly close to B3LYP

Table 5. Average Dihedral Angles and Dipole Moments of Various Conformers of Models **D**−**F** at Different QM Levels[a]

		dipole moment		av dihedral angles (SCC[b])					
model	structure	SCC[b]	B3LYP[c]	ϕ_1	θ_1	ψ_1	ϕ_2	θ_2	ψ_2
D	10/12/10/12/10	4.7	4.9	88.7	60.2	−107.1	−100.9	59.0	74.2
	12/10/12/10/12	1.2	1.8	−104.9	57.6	86.8	96.7	59.3	−125.8
	14-helix[d]	25.1	28.5	−134.3	60.0	−139.9			
	14-helix[e]	26.2	29.8	−141.9	61.4	−137.4			
	14-helix [f]	7.9	9.0						
E	10/12/10/12/10	3.5	3.7	71.7	62.9	−106.1	−103.7	60.4	85.0
	12/10/12/10/12	1.9	2.0	−104.1	59.6	99.1	75.4	64.3	−131.6
	14-helix[d]	25.0	27.9	−134.3	60.0	−139.9			
	14-helix[e]	25.8	28.8	−144.4	59.9	−135.3			
	14-helix [f]	16.5	18.2						
F	10/12/10/12/10	5.1	5.5	89.2	59.6	−106.4	−101.0	58.2	74.2
	12/10/12/10/12	2.1	2.8	110.0	−52.9	−88.9	−104.1	−56.7	113.6
	14-helix[d]	25.0	28.4	−134.3	60.0	−139.9			
	14-helix[e]	25.8	29.1	−144.1	59.2	−134.0			
	14-helix [f]	16.5	18.5						

[a] Dihedral angles in degrees and dipole moments in Debyes. [b] The standard parametrization of SCC-DFTB.[41] [c] B3LYP/6-31+G** at standard SCC-DFTB optimized structure. [d] Optimized with the backbone dihedral angles constrained to be ideal 14-helix values. [e] Optimized with the backbone dihedral angles constrained to be HF/6-31G* optimized values of Wu et al.[29] [f] Fully optimized without any constraints; for these structures, the average dihedral angles are less meaningful due to the substantial deviation from the ideal helical form and, therefore, not given.

Table 6. Relative Energies of Various Conformers of Models **D**−**F** at Different QM Levels[a]

model	structure	SCC[b]	SCC-dispersion[c]	SCC-Hbond[d]	B3LYP[e]	LMP2 [f]
D	10/12/10/12/10	0.0 (0.0)	0.0	0.0	0.0 (0.0)	0.0 (0.0)
	12/10/12/10/12	0.8 (0.1)	1.0	1.1	−3.9 (−1.3)	−3.5 (−1.4)
	14-helix[g]	32.5 (19.4)	35.8	34.8	21.0 (22.6)	21.6 (22.5)
	14-helix[h]	25.4 (19.4)	27.1	27.2	15.5 (22.6)	15.7 (22.5)
	14-helix[i]	9.4 (9.9)	7.4	10.0	12.5 (12.2)	12.4 (10.9)
E	10/12/10/12/10	0.0 (0.0)	0.0	0.0	0.0 (0.0)	0.0 (0.0)
	12/10/12/10/12	1.6 (1.4)	1.9	1.8	0.3 (−1.3)	−1.8 (0.04)
	14-helix[g]	26.2 (13.9)	28.9	27.9	11.4 (12.2)	5.4 (9.6)
	14-helix[h]	20.0 (13.9)	22.1	21.7	5.8 (12.2)	0.6 (9.6)
	14-helix[i]	13.0 (11.9)	16.1	14.0	9.2 (11.0)	5.2 (9.7)
F	10/12/10/12/10	0.0 (0.0)	0.0	0.0	0.0 (0.0)	0.0 (0.0)
	12/10/12/10/12	2.5 (3.8)	1.4	2.2	6.9 (8.5)	2.8 (4.0)
	14-helix[g]	31.9 (20.5)	34.1	33.8	21.3 (22.9)	17.4 (18.7)
	14-helix[h]	25.1 (20.5)	26.7	27.0	15.1 (22.9)	11.7 (18.7)
	14-helix[i]	17.2 (16.8)	18.7	18.3	20.5 (19.5)	17.7 (13.9)

[a] Energies are in kcal/mol; values in parentheses are computed using the B3LYP/6-31G* optimized structures, and others are computed using the standard SCC-DFTB optimized structures. [b] The standard parametrization of SCC-DFTB.[41] [c] SCC-DFTB with the empirical dispersion interaction.[68] [d] SCC-DFTB with the hydrogen-bonding interaction correction.[66,67] [e] B3LYP/6-31+G** energies. [f] LMP2/6-311G** energies. [g] Optimized with the backbone dihedral angles constrained to be ideal 14-helix values. [h] Optimized with the backbone dihedral angles constrained to be HF/6-31G* optimized values of Wu et al.[29] [i] Fully optimized without any constraints.

and LMP2 values; the rms errors of 10 degrees (Table 3) are expected considering the rather flat energy profiles along these torsional angles. The hydrogen-bonding correction for SCC-DFTB[66,67] changes the optimized structure only slightly with a rms in the dihedral angles of 6.6°. Dispersion also has only little effect on the geometries, based on results from both SCC-DFTB calculations that include the empirical dispersion[68] and LMP2 calculations.

For both **B** and **C**, the central torsional angle, θ, prefers the *gauche* conformation, and conformers with 8- and 6-membered hydrogen-bonding cycles are most stable. At all SCC-DFTB levels (i.e., regardless of hydrogen-bonding and dispersion effects), the global minimum is a C_8 conformer (**B1, C1**), although a C_6 conformer (**B2, C2**) is only slightly higher in energy by 0.2−0.6 kcal/mol. B3LYP and LMP2 calculations tend to favor the C_6 conformer, although the energy preference is again very small, on the order of 0.2−0.4 kcal/mol (see Tables 1 and 2).

Overall, there is very good agreement between SCC-DFTB, B3LYP, and LMP2 relative energies. Both hydrogen-bonding correction and dispersion have, in general, little effect on the SCC-DFTB results; in a few cases, however, including the dispersion causes certain conformers to disappear as local minima, often in agreement with the LMP2 result (see footnotes of Tables 1 and 2). The rms errors of the various SCC-DFTB models relative to the LMP2 results are 1.2−1.3 kcal/mol, only slightly larger than the value of 0.9 kcal/mol for B3LYP (Table 4). The major exception is **C11**, which adopts the 10/12 helical structure; it is 7.6 kcal/mol and 10 kcal/mol higher than the global minimum at the

LMP2 and B3LYP level, respectively, but is only ~3 kcal/mol higher than the global minimum at all SCC-DFTB levels.

For dipole moments, the SCC-DFTB results deviate from the B3LYP/6-31+G** values by ~15%, and the rms error is 0.9 Debye.

3. Conformational Studies of Heptapeptides. For the three heptapeptides, **D**−**F**, we focus on the three typical helical forms that have been studied in the previous work of Wu and Wang:[29] the 10/12 mixed helices (10/12/10/12/10, 12/10/12/10/12) and the 14-helix. For the 10/12 mixed helices, SCC-DFTB optimizations give structures (Table 5) in close agreement with both previous HF/6-31G*[29] and current B3LYP calculations, regardless of the hydrogen-bonding correction and inclusion of dispersion. For example, the rms difference in the dihedral angles is about 9 degrees relative to B3LYP/6-31G* calculations (Table 3), and the rmsd of backbone atoms is normally less than 0.2 Å. In addition, single point energies at both the B3LYP and LMP2 levels at the fully optimized SCC-DFTB structures are generally very similar to those at the B3LYP optimized structures (Table 6), indicating that the SCC-DFTB geometries are close to the B3LYP ones. As a result, as seen in Table 5, the conformational dependences in the dipole moment for all three heptapeptides are well reproduced at the SCC-DFTB level with a systematic underestimate of about 10%. The dipole moments of 14-helices are much greater than those of the 10/12 mixed helices, which makes the former better stabilized in polar solvent as found experimentally.[4,6,7]

Regarding energetics, SCC-DFTB systematically predicts the 10/12/10/12/10 helix to be lower in energy, although the preference over the 12/10/12/10/12 structure is smaller than 2 kcal/mol. At the B3LYP and LMP2 levels, the 12/10/12/10/12 form is lower in energy for **D** and **E**, although the preference is also very small and around 1 kcal/mol. For **F**, the LMP2 result is in fact closer to the SCC-DFTB results compared to the B3LYP value.

The situation for the 14 helical form is more complex. Figures 6−8 compare the structures obtained from various methods. For all three heptapeptides, the ideal 14-helix is not stable at the standard SCC-DFTB level and either partially converts to a 10- or 12-membered-ring hydrogen-bonding pattern or adopts bifurcated hydrogen-bonding at the two termini. Indeed, partial SCC-DFTB optimizations with the backbone dihedrals constrained to either the values in an ideal 14-helix or those in the reported HF/6-31G* structures of Wu and Wang[29] give structures of substantially higher energy than the fully optimized SCC-DFTB structures (Table 4). At the B3LYP/6-31G* level, the HF structures of Wu and Wang[29] do exist as stable local minima, although their energies are also higher than the structures optimized using the SCC-DFTB result as the starting configuration; this trend is maintained with LMP2/6-311G** single point energy calculations at the B3LYP geometries (Table 6). The B3LYP and SCC-DFTB optimized structures are generally very similar with backbone rmsd less than 0.4 Å, although B3LYP and LMP2 single point energies at the fully optimized SCC-DFTB structures tend to be *higher* than those at the partially optimized SCC-DFTB structures with backbone dihedrals constrained to the HF/6-31G* values, in contrast to both SCC-DFTB energies and high-level single point energies at the B3LYP optimized structures. This subtlety suggests that there are still non-negligible errors in the SCC-DFTB geometries, and caution has to be exercised when attempting to improve the energetics by performing high-level energy calculations at the SCC-DFTB structures.

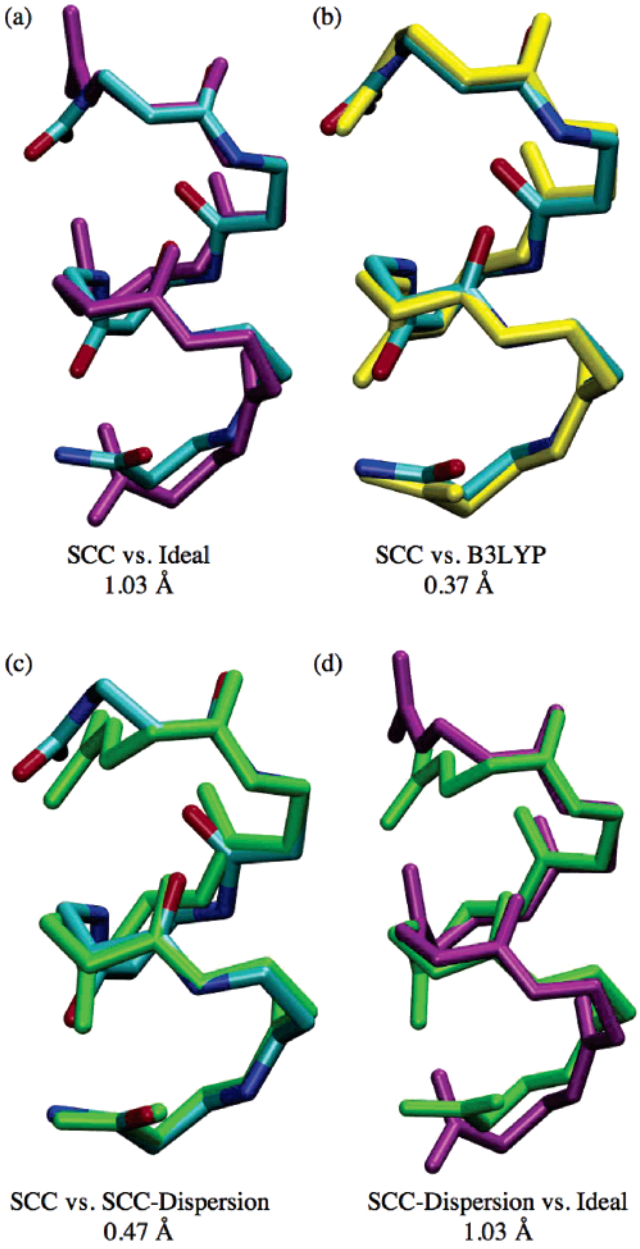

Figure 6. Comparison of different structures of model **D** from different calculations (the number below each superposition is the backbone rmsd): (a) SCC-DFTB optimized structure (CPK color) vs ideal 14-helix (purple); (b) SCC-DFTB optimized structure (CPK color) vs B3LYP/6-31G* optimized structure (yellow); (c) SCC-DFTB optimized structure (CPK color) vs SCC-DFTB+dispersion optimized structure (green); and (d) SCC-DFTB+dispersion optimized structure (green) vs ideal 14-helix (purple).

In general, the hydrogen-bonding correction to SCC-DFTB does not change the geometry or energetics of the heptapeptides studied here. By contrast, including dispersion gives more variations. Although dispersion does not affect the geometries of the 10/12 mixed helices, notable effects on

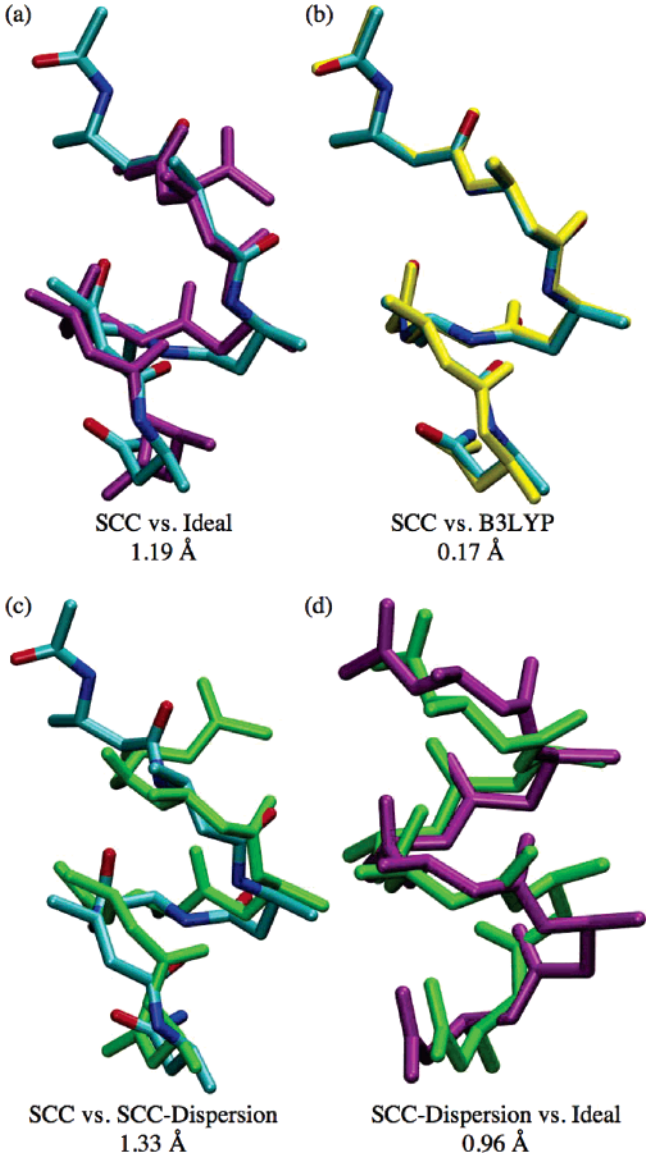

Figure 7. Comparison of different structures of model **E** from different calculations (the number below each superposition is the backbone rmsd): (a) SCC-DFTB optimized structure (CPK color) vs ideal 14-helix (purple); (b) SCC-DFTB optimized structure (CPK color) vs B3LYP/6-31G* optimized structure (yellow); (c) SCC-DFTB optimized structure (CPK color) vs SCC-DFTB+dispersion optimized structure (green); and (d) SCC-DFTB+dispersion optimized structure (green) vs ideal 14-helix (purple).

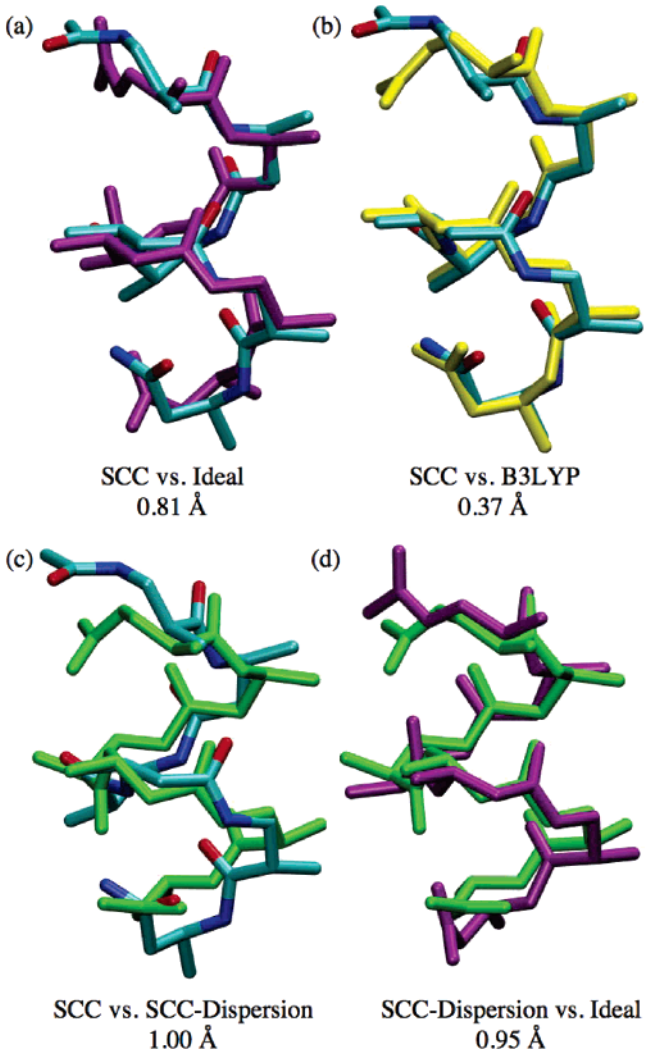

Figure 8. Comparison of different structures of model **F** from different calculations (the number below each superposition is the backbone rmsd): (a) SCC-DFTB optimized structure (CPK color) vs ideal 14-helix(purple); (b) SCC-DFTB optimized structure (CPK color) vs B3LYP/6-31G* optimized structure (yellow); (c) SCC-DFTB optimized structure (CPK color) vs SCC-DFTB+dispersion optimized structure(green); and (d) SCC-DFTB+dispersion optimized structure (green) vs ideal 14-helix (purple).

the structure of the 14-helix is observed except for **D**. For the β-substituted model **E**, with dispersion included in the SCC-DFTB, 14-membered-ring hydrogen bonds are formed except at the C terminus; the average dihedral angles for the 4 middle residues are $\phi = -160.5°$, $\theta = 61.0°$, and $\psi = -127.8°$, very close to the values in an ideal 14-helix.[2] Without dispersion, the two hydrogen bonds close to the C-terminus are completely lost, which leads to a structure with a rmsd value larger than 1.1 Å relative to the ideal 14-helix (Figure 7). For the mixed-substituted model **F**, by contrast, dispersion does not stabilize the ideal 14-helical structure (Figure 8). On average (Table 6), including dispersion *raises* the energy of the 14-helix relative to the 10/12 mixed helices by a small amount, which is somewhat unexpected based on the previous findings for natural peptides that dispersion stabilizes the wider α-helix than the thinner 3_{10}-helix.[69] This is probably because the larger number of atoms in the β-amino acids causes dispersion to saturate more quickly as a function of the number of residues compared to natural peptides, which leads to a smaller effect on the relative energies of different helical forms.

Overall, the findings from the heptapeptide calculations are similar to that for the dipeptides, which show that the standard SCC-DFTB parametrization gives rather reliable structures and relative energetics (rms error on the order of 2−3 kcal/mol) for various conformers as compared to B3LYP and LMP2 calculations. Therefore, it seems that the standard SCC-DFTB, even without the hydrogen-bonding correction[66,67] and dispersion interactions,[68] can describe the

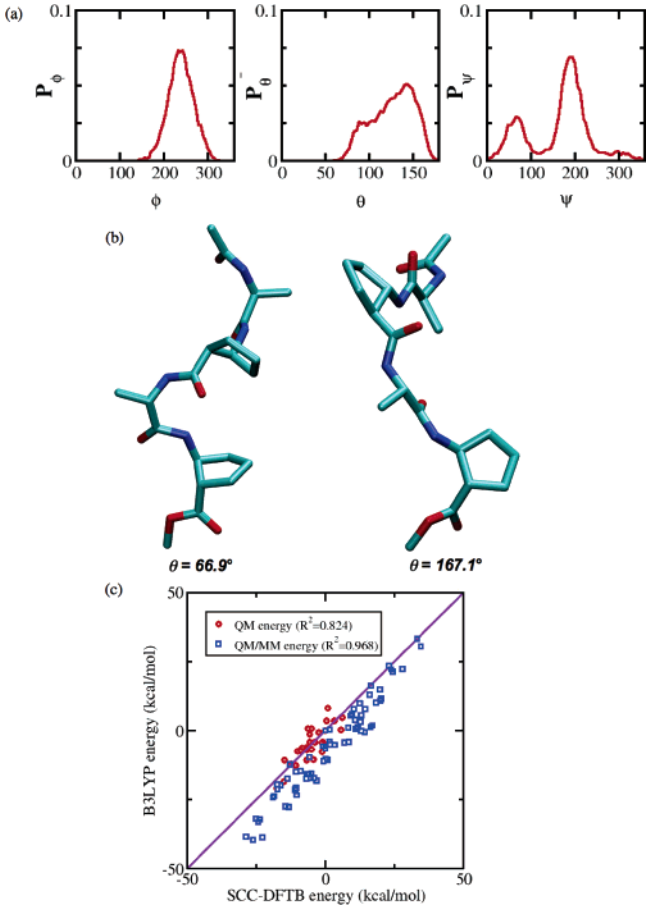

Figure 9. SCC-DFTB/MM simulations for the tetrapeptide (ACPC-A-ACPC-A) in water solution: (a) dihedral angle ϕ, θ, and ψ distributions of the central β-residue (ACPC); (b) two representitive snapshots with large and small θ angles; and (c) the correlation between SCC-DFTB/MM and B3LYP/6-31+G**/MM energies for ~70 snapshots taken from 2 ns SCC-DFTB/MM simulation (blue squares); gas-phase SCC-DFTB and B3LYP/6-31+G** energy correlations at those structures (red circles) are also shown for comparison.

intrinsic structural-energy relation of the helical forms of β-peptides to a satisfactory degree.

B. α/β-Mixed Peptides in the Condensed Phase. *1. Tetrapeptide (ACPC-A-ACPC-A) in Explicit Water*. The SCC-DFTB/MM simulations predict that the tetrapeptide is rather flexible, despite the five-membered ring in the β-amino acids: A wide range of θ values are sampled within a time duration of 2 ns. The conformational properties of the tetrapeptide and comparison with ab initio calculations are presented in Figure 9. The probability distribution function for θ is weakly bimodal with two peaks (Figure 9a). Characteristic structures corresponding to the values of θ at the peak in the distribution are rather different (Figure 9b). The ϕ and ψ predominately sample the region that corresponds to the β-sheet structure of α-peptides in the Ramachandran plot.[83] Evidently, different ϕ-ψ ranges characterize secondary structures in non-natural peptides.

To further validate the SCC-DFTB/MM model, a number of randomly chosen snapshots (~70) are taken from the SCC-DFTB/MM trajectory, and single point energies are calculated at the B3LYP/6-31+G**/MM level. As seen in Figure 9c, the SCC-DFTB/MM energies show a good correlation with the B3LYP/MM results with a correlation coefficient of 0.968, although SCC-DFTB/MM systematically underestimates the relative energies. Interestingly, the correlation is weaker when only gas-phase energies at the same structures are considered (i.e., without the interaction with the MM water molecules), which has a correlation coefficient of 0.824. Apparently, there is some degree of cancellation between the gas-phase errors in SCC-DFTB and the errors associated with the QM/MM interactions in the SCC-DFTB/MM framework; the SCC-DFTB/MM interaction is treated with the same Mulliken approximation as for the electrostatic interactions between SCC-DFTB atoms, while the QM/MM interactions are calculated with exact one-electron integrals in the B3LYP/MM calculations.[74] Considering the wide range of conformations sampled in the SCC-DFTB/MM simulations, the general agreement with B3LYP/MM energies is encouraging.

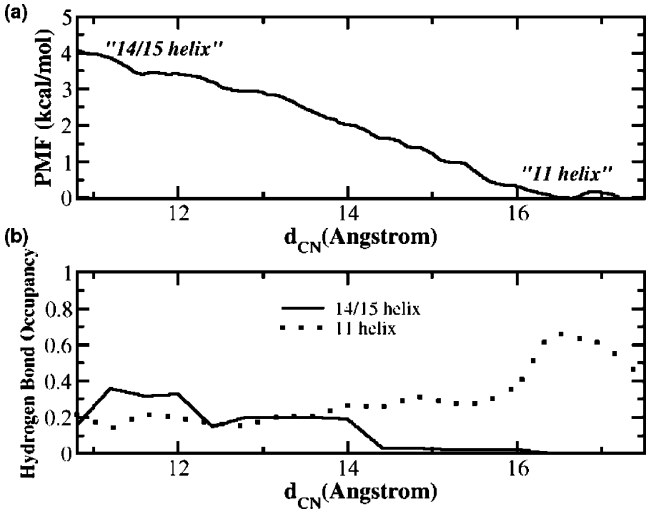

Figure 10. SCC-DFTB/MM simulations for octapeptide (ACPC-A-ACPC-A-ACPC-A-ACPC-A) in methanol solution: (a) PMF for the conversion between the 14/15-helix and 11-helix of octapeptide and (b) hydrogen-bonding occupancy analysis (solid line: 14/15-helix; dashed line: 11-helix).

2. Octapeptide (ACPC-A-ACPC−ACPC-A-ACPC-A) in Methanol. For the octapeptide in methanol, the key question is the relative stability of the 14/15 and 11 helices. Experiments[10] suggest that both of these structures are present with detectable populations, although a quantitative characterization was not reported. Figure 10(a) depicts the potential of mean force for the conversion between the 14/15-helix and the 11-helix. The SCC-DFTB/MM simulations (Figure 10a) show that the 11-helix is more stable than the 14/15-helix by about 3 kcal/mol. If we consider that the gas-phase calculations discussed above suggest that SCC-DFTB tends to underestimate the stability of shorter and wider helices (e.g., the stability of the 14-helix is underestimated compared to 10/12 mixed helices for heptapeptides in Table 4), the PMF result implies that the two helical forms are even closer in free energy (14/15-helix is shorter and wider than the 11-helix) than 3 kcal/mol, which is qualitatively consistent with the experimental NOE data.[10]

The order parameter used in the PMF calculations, d_{CN}, appears to be a valid one since it can effectively distinguish

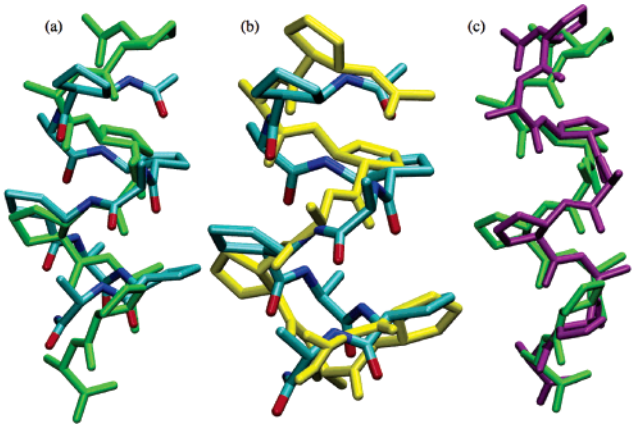

Figure 11. Structures of 14/15 and 11 helices of octapeptide (ACPC-A-ACPC-A-ACPC-A-ACPC-A) in methanol: (a) superposition of the ideal 14/15-helix (CPK color) and 11-helix (green); (b) superposition of the ideal 14/15-helix (CPK color) and the average structure of the window $d_{CN} = 11.4$ Å; and (c) superposition of the ideal 11-helix (green) and the average structure of the window $d_{CN} = 17.0$ Å (purple).

the two helical forms based on the average structures from different windows (Figure 11). There is an interesting difference in the stability of the backbone hydrogen-bonding interactions between the two helical forms (Figure 10b). Although the occupancy of the backbone hydrogen bonds is rather high (~0.7) for the 11-helix, the value is substantially lower (<0.4) for the 14/15-helix, implying a very dynamical structure for the latter.

IV. Conclusions and Outlook

Carrying out molecular simulations of non-natural peptides is both exciting and challenging. On one hand, the lack of extensive amount of experimental data means that molecular simulations can play a major role in understanding the structural and dynamical properties of these novel materials. On the other hand, there is only a limited amount of data available for establishing a robust molecular model and simulation protocol. Our long-term goal is to use QM/MM models to guide the development of classical models for β- and α/β-peptides at both the all-atom and coarse-grained levels, such that the relationship between the sequence of these peptides and their structural as well as material properties can be analyzed. This is motivated by the fact that the reliability of a QM model can be meaningfully tested in both the gas phase and condensed phase by comparing to high-level QM calculations and available experimental data, respectively.

In this paper, the reliability of an approximate density functional theory, SCC-DFTB, as the QM model for β- and α/β-mixed peptides has been tested by both gas-phase and condensed-phase calculations for several rather different systems. In the gas phase, both cyclic and acyclic dipeptides and three acyclic heptapeptides have been studied at several QM levels, including the standard SCC-DFTB, B3LYP, and LMP2; the effect of two recent enhancements to SCC-DFTB, which deal with hydrogen-bonding interactions and dispersion interactions, has also been tested. Overall, the standard SCC-DFTB approach has been shown to reproduce the B3LYP structures with an rms error in the key dihedral angles of less than 14 degrees. Importantly, SCC-DFTB is able to capture the lowest-energy conformers for all dipeptides and heptapeptides studied here, although several local minima of higher energy, such as the ideal 14-helical form for the heptapeptides, are missed at the SCC-DFTB level. The relative energies of different conformers are also well described in general, with typical rms errors of 2−3 kcal/mol relative to LMP2 single points at the B3LYP structures. The dipole moments are reproduced with a systematic underestimate of approximately 15%. The effect of including the hydrogen-bonding correction or empirical dispersion in the SCC-DFTB calculations is generally small, although including dispersion in several cases leads to rather different structures; the effect of those corrections is expected to be more significant when comparing folded (compact) structures and unfolded structures, as found in the folding simulation of β-peptides (Zhu, X. et al., work in progress). In addition to the gas-phase studies, SCC-DFTB/MM simulations have been carried out for a tetra-α/β-mixed peptide in water and for an octamer in methanol. For the tetrameric system, the SCC-DFTB/MM energies are well correlated with B3LYP/6-31+G**/MM single point energies for a wide range of structures sampled in 2 ns of SCC-DFTB/MM molecular dynamics trajectory. For the octamer, PMF calculations indicate that the 14/15 and 11 helices are within 3 kcal/mol in free energy with the latter being more stable, which is in qualitative agreement with available NOE data.

With all these results taken together, it is established that although SCC-DFTB has non-negligible errors in structures and energetics compared to high-level DFT and ab initio methods, it is expected to capture the most important configurations for β- and α/β-mixed peptides. Considering their computational efficiency, we conclude that SCC-DFTB and SCC-DFTB/MM are effective methods for describing the structure-energy properties of these non-natural peptides in the gas phase and solution (water, methanol) phase, respectively. In particular, SCC-DFTB/MM simulations can be used as the unique reference for developing useful MM models at multiple resolutions. Such studies are in progress.

Acknowledgment. This work is supported from the National Science Foundation (CRC-CHE-0404704). Discussions with Prof. S. Gellman, Dr. M. Schmitt, and Mr. S. H. Choi are greatly appreciated. Q.C. also acknowledges an Alfred P. Sloan Research Fellowship. Computational resources from the National Center for Supercomputing Applications at the University of Illinois are greatly appreciated.

Supporting Information Available: Calculations for the bulk properties of methanol using two different classical force field models, comparison to experimental results, and the complete ref 36. This material is available free of charge via the Internet at http://pubs.acs.org.

References

(1) Gellman, S. H. *Acc. Chem. Res.* **1998**, *31*, 173−180.

(2) Cheng, R. P.; Gellman, S. H.; DeGrado, W. F. *Chem. Rev.* **2001**, *101*, 3219−3232.

(3) DeGrado, W. F.; Schneider, J. P.; Hamuro, Y. *J. Peptide Res.* **1999**, *54*, 206−217.

(4) Appella, D. H.; Christianson, L. A.; Karle, I. L.; Powell, D. R.; Gellman, S. H. *J. Am. Chem. Soc.* **1996**, *118*, 13071−13072.

(5) Appella, D. H.; Christianson, L. A.; Klein, D. A.; Richards, M. R.; Powell, D. R.; Gellman, S. H. *J. Am. Chem. Soc.* **1999**, *121*, 7574−7581.

(6) Appella, D. H.; Christianson, L. A.; Karle, I. L.; Powell, D. R.; Gellman, S. H. *J. Am. Chem. Soc.* **1999**, *121*, 6206−6212.

(7) Seebach, D.; Overhand, M.; Kühnle, F. N. M.; Martinoni, B.; Oberer, L.; Hommel, U.; Widmer, H. *Helv. Chim. Acta* **1996**, *79*, 913−941.

(8) Seebach, D.; Gademann, K.; Schreiber, J. V.; Matthews, J. L.; Hintermann, T.; Jaun, B.; Oberer, L.; Hommel, U.; Widmer, H. *Helv. Chim. Acta* **1997**, *80*, 2033−2038.

(9) Hayen, A.; Schmitt, M. A.; Ngassa, F. N.; Thomasson, K. A.; Gellman, S. H. *Angew. Chem., Int. Ed.* **2004**, *43*, 505−510.

(10) Schmitt, M. A.; Choi, S. H.; Guzei, I. A.; Gellman, S. H. *J. Am. Chem. Soc.* **2005**, *127*, 13130−13131.

(11) Porter, E. A.; Wang, X. F.; Lee, H. S.; Weisblum, B.; Gellman, S. H. *Nature* **2000**, *404*, 565−565.

(12) Porter, E. A.; Weisblum, B.; Gellman, S. H. *J. Am. Chem. Soc.* **2002**, *124*, 7324−7330.

(13) Raguse, T. L.; Porter, E. A.; Weisblum, B.; Gellman, S. H. *J. Am. Chem. Soc.* **2002**, *124*, 12774−12785.

(14) Hamuro, Y.; Schneider, J. P.; DeGrado, W. F. *J. Am. Chem. Soc.* **1999**, *121*, 12200−12201.

(15) Liu, D. H.; DeGrado, W. F. *J. Am. Chem. Soc.* **2001**, *123*, 7553−7559.

(16) Schmitt, M. A.; Weisblum, B.; Gellman, S. H. *J. Am. Chem. Soc.* **2004**, *126*, 6848−6849.

(17) Eldred, S. E.; Pancost, M. R.; Otte, K. M.; Rozema, D.; Stahl, S. S.; Gellman, S. H. *Bioconjugate Chem.* **2005**, *16*, 694−699.

(18) Wu, C. W.; Seurynck, S. L.; Lee, K. Y. C.; Barron, A. E. *Chem. Biol.* **2003**, *11*, 1057−1063.

(19) Glättli, A.; Daura, X.; Seebach, D.; van Gunsteren, W. F. *J. Am. Chem. Soc.* **2002**, *124*, 12972−12978.

(20) Seebach, D.; Ciceri, P. E.; Overhand, M.; Jaun, B.; Rigo, D.; Oberer, L.; Hommel, U.; Amstutz, R.; Widmer, H. *Helv. Chim. Acta* **1996**, *79*, 2043−2066.

(21) Arvidsson, P. I.; Rueping, M.; Seebach, D. *Chem. Commun.* **2001**, 649−650.

(22) Cheng, R. P.; DeGrado, W. F. *J. Am. Chem. Soc.* **2001**, *123*, 5162−5163.

(23) Cheng, R. P.; DeGrado, W. F. *J. Am. Chem. Soc.* **2002**, *124*, 11564−11565.

(24) Hart, S. A.; Bahadoor, A. B. F.; Matthews, E. E.; Qiu, X. Y. J.; Schepartz, A. *J. Am. Chem. Soc.* **2003**, *125*, 4022−4023.

(25) Raguse, T. L.; Lai, J. R.; Gellman, S. H. *Helv. Chim. Acta* **2002**, *85*, 4154−4164.

(26) Glättli, A.; Seebach, D.; van Gunsteren, W. F. *Helv. Chim. Acta* **2004**, *87*, 2487−2506.

(27) Baldauf, C.; Günther, R.; Hofmann, H. J. *Biopolymers* **2006**, *84*, 408−413.

(28) Wu, Y. D.; Wang, D. P. *J. Am. Chem. Soc.* **1998**, *120*, 13485−13493.

(29) Wu, Y. D.; Wang, D. P. *J. Am. Chem. Soc.* **1999**, *121*, 9352−9362.

(30) Möhle, K.; Günther, R.; Thormann, M.; Sewald, N.; Hofmann, H. J. *Biopolymers* **1999**, *50*, 167−184.

(31) Appella, D. H.; Christianson, L. A.; Klein, D. A.; Powell, D. R.; Huang, X. L.; Barchi, J. J.; Gellman, S. H. *Nature* **1997**, *387*, 381−384.

(32) Daura, X.; van Gunsteren, W. F.; Rigo, D.; Jaun, B.; Seebach, D. *Chem. Eur. J.* **1997**, *3*, 1410−1417.

(33) Daura, X.; Jaun, B.; Seebach, D.; van Gunsteren, W. F.; Mark, A. E. *J. Mol. Biol.* **1998**, *280*, 925−932.

(34) Daura, X.; van Gunsteren, W. F.; Mark, A. E. *Proteins: Struct., Funct., Genet.* **1999**, *34*, 269−280.

(35) Glättli, A.; Daura, X.; Bindschadler, P.; Jaun, B.; Mahajan, Y. R.; Mathad, R. I.; Rueping, M.; Seebach, D.; vanGunsteren, W. F. *Chem. Eur. J.* **2005**, *11*, 7276−7293.

(36) MacKerell, A. D., Jr.; et al.; Karplus, M. *J. Phys. Chem. B* **1998**, *102*, 3586−3616.

(37) Field, M. J.; Bash, P. A.; Karplus, M. *J. Comput. Chem.* **1990**, *11*, 700−733.

(38) Gao, J. *Methods and Applications of Combined Quantum Mechanical and Molecular Mechanical Potentials*; VCH: New York, 1995; Vol. 7 of *Reviews in Computational Chemistry*.

(39) Shurki, A.; Warshel, A. *Adv. Prot. Chem.* **2003**, *66*, 249.

(40) Friesner, R. A.; Guallar, V. *Annu. Rev. Phys. Chem.* **2005**, *56*, 389−427.

(41) Elstner, M.; Porezag, D.; Jungnickel, G.; Elsner, J.; Haugk, M.; Frauenheim, T.; Suhai, S.; Seifert, G. *Phys. Rev. B* **1998**, *58*, 7260−7268.

(42) Kolb, M.; Thiel, W. *J. Comput. Chem.* **1993**, *14*, 775−789.

(43) Elstner, M.; Jalkanen, K. J.; Knapp-Mohammady, M.; Frauenheim, T.; Suhai, S. *Chem. Phys.* **2001**, *263*, 203−219.

(44) Elstner, M.; Jalkanen, K. J.; Knapp-Mohammady, M.; Frauenheim, T.; Suhai, S. *Chem. Phys.* **2000**, *256*, 15−27.

(45) Hu, H.; Elstner, M.; Hermans, J. *Proteins: Struct., Funct., Genet.* **2003**, *50*, 451−463.

(46) Cui, Q.; Elstner, M.; Kaxiras, E.; Frauenheim, T.; Karplus, M. *J. Phys. Chem. B* **2001**, *105*, 569−585.

(47) Zhang, X.; Harrison, D.; Cui, Q. *J. Am. Chem. Soc.* **2002**, *124*, 14871−14878.

(48) Li, G.; Cui, Q. *J. Am. Chem. Soc.* **2003**, *125*, 15028−15038.

(49) Bondar, A. N.; Fischer, S.; Smith, J. C.; Elstner, M.; Suhai, S. *J. Am. Chem. Soc.* **2004**, *126*, 14668−14677.

(50) Elstner, M.; Frauenheim, T.; Suhai, S. *THEOCHEM* **2003**, *632*, 29.

(51) Kruger, T.; Elstner, M.; Schiffels, P.; Frauenheim, T. *J. Chem. Phys.* **2005**, *122*, 114110.

(52) Elstner, M.; Hobza, P.; Frauenheim, T.; Suhai, S.; Kaxiras, E. *J. Chem. Phys.* **2001**, *114*, 5149−5155.

(53) Liu, H.; Elstner, M.; Kaxiras, E.; Frauenheim, T.; Hermans, J.; Yang, W. *Proteins* **2001**, *44*, 484.

(54) Parr, R. G.; Yang, W. T. *Density-Functional Theory of Atoms and Molecules*; Oxford University Press: New York, 1989.

(55) Saebo, S.; Pulay, P. *Annu. Rev. Phys. Chem.* **1993**, *44*, 213−236.

(56) Petersson, G. A.; Bennett, A.; Tensfeldt, T. G.; Allaham, M. A.; Shirley, W. A.; Mantzaris, J. *J. Chem. Phys.* **1988**, *89*, 2193−2218.

(57) Becke, A. D. *Phys. Rev. A* **1988**, *38*, 3098−3100.

(58) Becke, A. D. *J. Chem. Phys.* **1993**, *98*, 5648−5652.

(59) Lee, C. T.; Yang, W. T.; Parr, R. G. *Phys. Rev. B* **1988**, *37*, 785−789.

(60) Krishnan, R.; Binkley, J. S.; Seeger, R.; Pople, J. A. *J. Chem. Phys.* **1980**, *72*, 650−654.

(61) Florian, J.; Johnson, B. G. *J. Phys. Chem.* **1995**, *99*, 5899−5908.

(62) Lii, J. H.; Ma, B. Y.; Allinger, N. L. *J. Comput. Chem.* **1999**, *20*, 1593−1603.

(63) Saebo, S.; Tong, W.; Pulay, P. *J. Chem. Phys.* **1993**, *98*, 2170−2175.

(64) Murphy, R. B.; Beachy, M. D.; Friesner, R. A.; Ringnalda, M. N. *J. Chem. Phys.* **1995**, *103*, 1481−1490.

(65) Beachy, M. D.; Chasman, D.; Murphy, R. B.; Halgren, T. A.; Friesner, R. A. *J. Am. Chem. Soc.* **1997**, *119*, 5908−5920.

(66) Riccardi, D.; Schaefer, P.; Yang, Y.; Yu, H.; Ghosh, N.; Prat-Resina, X.; König, P.; Xu, D.; Guo, H.; Elstner, M.; Cui, Q. *J. Phys. Chem. B* **2006**, *110*, 6458−6469.

(67) Elstner, M. *Theor. Chem. Acc.* **2006**, *116*, 316−325.

(68) Elstner, M.; Hobza, P.; Frauenheim, T.; Suhai, S.; Kaxiras, E. *J. Chem. Phys.* **2001**, *114*, 5149−5155.

(69) Wu, Q.; Yang, W. T. *J. Chem. Phys.* **2002**, *116*, 515−524.

(70) Kristyan, S.; Pulay, P. *Chem. Phys. Lett.* **1994**, *229*, 175−180.

(71) Frisch, M. J.; Pople, J. A. et al. *Gaussian 03, Revision B.05*; Gaussian, Inc.: Wallingford, CT, 2004.

(72) Schrödinger, L. L. C. *Jaguar 5.5*; New York, 1991−2006.

(73) Brooks, B. R.; Bruccoleri, R. E.; Olafson, B. D.; States, D. J.; Swaminathan, S.; Karplus, M. *J. Comput. Chem.* **1983**, *4*, 187−217.

(74) Cui, Q.; Elstner, M.; Kaxiras, E.; Frauenheim, T.; Karplus, M. *J. Phys. Chem. B* **2001**, *105*, 569−585.

(75) Jorgensen, W. L.; Chandrasekhar, J.; Madura, J. D.; Impey, R. W.; Klein, M. L. *J. Chem. Phys.* **1983**, *79*, 926−935.

(76) Im, W.; Berneche, S.; Roux, B. *J. Chem. Phys.* **2001**, *114*, 2924−2937.

(77) Schaefer, P.; Riccardi, D.; Cui, Q. *J. Chem. Phys.* **2005**, *123*, 014905.

(78) Brooks, C. L.; Karplus, M. *J. Chem. Phys.* **1983**, *79*, 6312−6325.

(79) Ryckaert, J. P.; Ciccotti, G.; Berendsen, H. J. C. *J. Comput. Phys.* **1977**, *23*, 327−341.

(80) Schmidt, M. W.; Baldridge, K. K.; Boatz, J. A.; Elbert, S. T.; Gordon, M. S.; Jensen, J. H.; Koseki, S.; Matsunaga, N.; Nguyen, K. A.; Su, S. J.; Windus, T. L.; Dupuis, M.; Montgomery, J. A. *J. Comput. Chem.* **1993**, *14*, 1347−1363.

(81) Torrie, G. M.; Valleau, J. P. *J. Comput. Phys.* **1977**, *23*, 187−199.

(82) Kumar, S.; Bouzida, D.; Swendsen, R. H.; Kollman, P. A.; Rosenberg, J. M. *J. Comput. Chem.* **1992**, *13*, 1011−1021.

(83) Ramachandran, G. N.; V. S. *Adv. Prot. Chem.* **1968**, *23*, 283−438.

CT600352E